

# Tuning the effective fine structure constant in graphene: opposing effects of dielectric screening on short- and long-range potential scattering

C. Jang<sup>1</sup>, S. Adam<sup>2</sup>, J.-H. Chen<sup>1,3</sup>, E. D. Williams<sup>1,3</sup>, S. Das Sarma<sup>1,2</sup> and M. S. Fuhrer<sup>1,3</sup>

<sup>1</sup>Center for Nanophysics and Advanced Materials,

<sup>2</sup>Condensed Matter Theory Center, and

<sup>3</sup>Materials Research Science and Engineering Center, Department of Physics,  
University of Maryland, College Park, MD 20742-4111, USA

(Dated: November 26, 2024)

We reduce the dimensionless interaction strength  $\alpha$  in graphene by adding a water overlayer in ultra-high vacuum, thereby increasing dielectric screening. The mobility limited by long-range impurity scattering is *increased* over 30 percent, due to the background dielectric constant enhancement leading to reduced interaction of electrons with charged impurities. However, the carrier-density-independent conductivity due to short range impurities is *decreased* by almost 40 percent, due to reduced screening of the impurity potential by conduction electrons. The minimum conductivity is nearly unchanged, due to canceling contributions from the electron/hole puddle density and long-range impurity mobility. Experimental data are compared with theoretical predictions with excellent agreement.

PACS numbers:

Most theoretical and experimental work on graphene has focused on its gapless, linear electronic energy dispersion  $E = \hbar v_F k$ . One important consequence of this linear spectrum is that the dimensionless coupling constant  $\alpha$  (or equivalently  $r_s$ , defined here as the ratio between the graphene Coulomb potential energy and kinetic energy) is a carrier-density independent constant [1, 2], and as a result, the Coulomb potential of charged impurities in graphene is renormalized by screening, but strictly maintains its long-range character. Thus there is a clear dichotomy between long-range and short-range scattering in graphene, with the former giving rise to a conductivity linear [2, 3] in carrier density (constant mobility), and the latter having a constant conductivity independent of carrier density. Charged impurity scattering necessarily dominates at low carrier density, and the minimum conductivity at charge neutrality is determined by the charged impurity scattering and the self-consistent electron and hole puddles of the screened impurity potential [3, 4, 5, 6].

Apart from the linear spectrum, an additional striking aspect of graphene, setting it apart from all other two-dimensional electron systems, is that the electrons are confined to a plane of atomic thickness. This fact has a number of ramifications which are only beginning to be explored [7]. One such consequence is that graphene's properties may be tuned enormously by changing the surrounding environment. Here we provide a clear demonstration of this by reducing the dimensionless coupling constant  $\alpha$  in graphene by more than 30 percent through the addition of a dielectric layer (ice) on top of the graphene sheet. Upon addition of the ice layer, the mobility limited by long-range scattering by charged impurities *increases* by 31 percent, while the conductivity limited by short-range scatterers *decreases* by 38 percent. The minimum conductivity value remains nearly unchanged. The

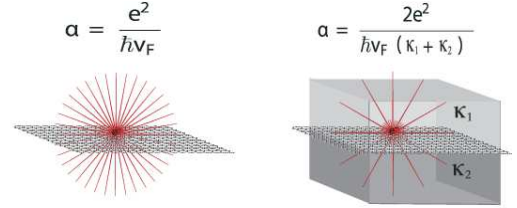


FIG. 1: Schematic illustrating dielectric screening in graphene. The dielectric environment controls in the interaction strength parameterized by the coupling constant  $\alpha$ .

opposing effects of reducing  $\alpha$  on short- and long-range scattering are easily understood theoretically. The major effect on long-range scattering is to reduce the Coulomb interaction of electrons with charged impurities, reducing the scattering [8]. In contrast, the dielectric does not modify the atomic-scale potential of short-range scatterers, and there the leading effect is the reduction of screening by the charge carriers, which increases scattering resulting in lower high-density conductivity. Such screening of short-range potentials has been predicted theoretically [9], although in other 2D systems, this effect is difficult to observe experimentally. The minimum conductivity is nearly unchanged due to competing effects of increased mobility and reduced carrier concentration in electron-hole puddles due to reduced screening [4, 10].

Fig. 1 illustrates the effect of the dielectric environment on graphene. For graphene sandwiched between two dielectric slabs with  $\kappa_1$  and  $\kappa_2$ ,

$$\alpha = \frac{2e^2}{(\kappa_1 + \kappa_2)\hbar v_F}, \quad (1)$$

where  $e$  is the electronic charge,  $\hbar$  is Planck's constant, and  $v_F$  is the Fermi velocity, which we take to

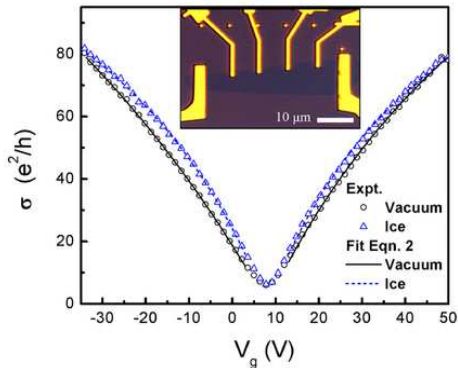


FIG. 2: (Color online) Conductivity of the graphene device as a function of back-gate voltage for pristine graphene (circles) and after deposition of 6 monolayers of ice (triangles). Lines are fits to Eq. 2. Inset: Optical microscope image of the device.

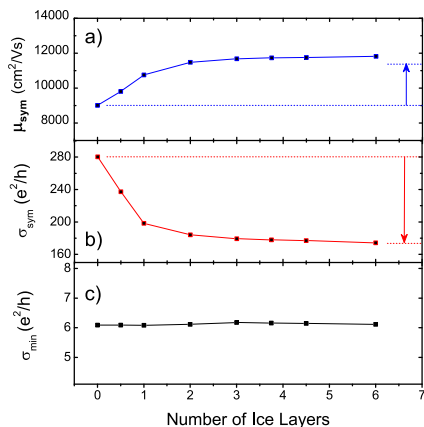


FIG. 3: (Color online)  $\mu_{\text{sym}}$ ,  $\sigma_{\text{sym}}$  and  $\sigma_{\text{min}}$  as a function of number of ice layers. Dashed lines show the values for pristine graphene and corresponding theoretical expectations for the ice-covered device.

be  $1.1 \times 10^6$  m/s [11, 12, 13]. Typically, graphene transport experiments [5, 6, 11, 12] are performed on a  $\text{SiO}_2$  substrate with  $\kappa_1 \approx 3.9$  and in air/vacuum  $\kappa_2 \approx 1$ , making graphene a weakly interacting electron system with  $\alpha \approx 0.8$  (although very recently work on substrate-free graphene [14] explored the strong coupling regime with  $\alpha \approx 2$ ). Here we deposit ice ( $\kappa_2 \approx 3.2$  [15]) on graphene on  $\text{SiO}_2$ , decreasing  $\alpha$  from  $\approx 0.81$  to  $\approx 0.56$ .

Graphene is obtained by mechanical exfoliation of Kish graphite on a  $\text{SiO}_2$  (300 nm)/Si substrate [11]. Graphene monolayers are identified from the color contrast in an optical microscope image and confirmed by Raman spectroscopy [16]. The final device (see Fig 2 inset) was fabricated by patterning electrodes using electron beam lithography and thermally evaporated Cr/Au, followed

by annealing in  $\text{Ar}/\text{H}_2$  to remove resist residue (see Refs. [6, 17] for details). The experiments are performed in a cryostat cold finger placed in an ultra high vacuum (UHV) chamber. In order to remove residual adsorbed gases on the device and the substrate, the sample was baked at 430 K over-night in UHV following a vacuum bakeout. The conductivity was measured using a conventional four-probe technique with an ac current of 50 nA at a base pressure ( $\sim 10^{-10}$  torr) and device temperature ( $\sim 77$  K). Deionized nano-pure water was introduced through a leak valve attached to the chamber. The water gas pressure (determined by a residual gas analyzer) was  $5 \pm 3 \times 10^{-8}$  torr. The amount of ice deposited was estimated by assuming a sticking coefficient of unity and the ice  $I_h$  layer density of  $9.54 \times 10^{14}$   $\text{cm}^{-2}$  [18, 19].

Fig. 2 shows conductivity as a function of gate voltage for two different sample conditions, pristine graphene and ice-covered graphene. We observe several interesting effects of adding ice: (i) The offset gate voltage at which the conductivity is a minimum  $V_{g,\text{min}}$  remains unchanged; (ii) the minimum conductivity  $\sigma_{\text{min}}$  value remains unchanged, (iii) the maximum slope of  $\sigma(V_g)$  becomes steeper, and (iv) the curve  $\sigma(V_g)$  in the presence of ice is more non-linear and crosses that of the pristine sample at some large carrier density. All these features can be understood qualitatively from the physical picture described above, and we show below that they are in quantitative agreement with the predictions of Boltzmann transport theory including screening within the Random Phase Approximation (RPA).

In order to interpret the experimental results quantitatively [21], we fit the conductivity data to

$$\sigma^{-1}(V_g, \alpha) = (ne\mu_i)^{-1} + (\sigma_s)^{-1}, \quad (2)$$

where  $n = c_g|V_g - V_{g,\text{min}}|$ ,  $e$  is the electric charge and  $c_g = 1.15 \times 10^{-8}$   $\text{V}/\text{cm}^2$  is the gate capacitance per unit area for the 300 nm thick  $\text{SiO}_2$ . Since the transport curves are not symmetric about the minimum gate voltage, the fitting is performed separately for positive and negative carrier densities (i.e. electron and hole carriers), excluding data close to the Dirac point conductivity plateau ( $V_{g,\text{min}} \pm 5\text{V}$ ). We report both the symmetric  $\mu_{\text{sym}}(\sigma_{\text{sym}})$  and antisymmetric  $\mu_{\text{asym}}(\sigma_{\text{asym}})$  contributions to the mobility (conductivity). Shown also in Fig. 2 is the result of the fit for pristine graphene and after deposition of 6 monolayers of ice.

Figure 3 shows  $\mu_{\text{sym}}$ ,  $\sigma_{\text{sym}}$  and  $\sigma_{\text{min}}$  as a function of number of ice layers. The mobility (Fig. 3a) of pristine graphene is 9,000  $\text{cm}^2/\text{Vs}$ , which is typical for clean graphene devices on  $\text{SiO}_2$  substrates at low temperature. As the number of water layers increases, the mobility *increases*, and saturates after about 3 layers of ice to about 12,000  $\text{cm}^2/\text{Vs}$ . In contrast, the conductivity due to short-range scatterers (Fig. 3b) decreases from 280  $e^2/h$

to  $170 e^2/h$ . The decrease in conductivity due to short-range scatterers shows a similar saturation behavior as the mobility, suggesting they have the same origin [20]. The absence of any sharp change in the conductivity or mobility at very low ice coverage rules out ice itself acting as a significant source of short- or long-range scat-

tering. This is corroborated by the absence of a shift in the gate voltage of the minimum conductivity, consistent with physisorbed ice [18] not donating charge to graphene [4, 5, 6]. Fig. 3c shows that the minimum conductivity is essentially unchanged during the addition of ice.

TABLE I: Summary of our results and corresponding theoretical predictions.

		Theory	Experiment
Long-range (symmetric): $\frac{\mu_{\text{sym}}^{\text{ice}}}{\mu_{\text{sym}}^{\text{vac}}} = \frac{F_l(\alpha^{\text{vac}})}{F_l(\alpha^{\text{ice}})}$	Ref. [4]	1.26	1.31
Short-range (symmetric): $\frac{\sigma_{\text{sym}}^{\text{ice}}}{\sigma_{\text{sym}}^{\text{vac}}} = \frac{F_s(\alpha^{\text{vac}})}{F_s(\alpha^{\text{ice}})}$	Ref. [22]	0.62	0.62
Minimum conductivity: $\frac{\sigma_{\text{min}}^{\text{ice}}}{\sigma_{\text{min}}^{\text{vac}}} = \frac{n^*(\alpha^{\text{ice}})F_l(\alpha^{\text{vac}})}{n^*(\alpha^{\text{vac}})F_l(\alpha^{\text{ice}})}$	Ref. [4]	0.99	1.00
Long-range (anti-symmetric): $\frac{\mu_{\text{asym}}^{\text{ice}}}{\mu_{\text{asym}}^{\text{vac}}} = \frac{F_l(\alpha^{\text{vac}})}{F_l(\alpha^{\text{ice}})} \frac{\alpha^{\text{ice}}}{\alpha^{\text{vac}}}$	Ref. [26]	0.87	0.17
Short-range (anti-symmetric): $\frac{\sigma_{\text{asym}}^{\text{ice}}}{\sigma_{\text{asym}}^{\text{vac}}}$	Ref. [27]		0.13

We now analyze the experimental results within Boltzmann transport theory. The conductivity of graphene depends strongly on the coupling constant  $\alpha$ . For screened long-range impurities within RPA, we have [4]

$$\begin{aligned} \sigma_l &= \frac{2e^2}{h} \frac{n}{n_{\text{imp}}} \frac{1}{F_l(\alpha)}, \\ F_l(\alpha) &= \pi\alpha^2 + 24\alpha^3(1 - \pi\alpha) \\ &\quad + \frac{16\alpha^3(6\alpha^2 - 1) \arccos[1/2\alpha]}{\sqrt{4\alpha^2 - 1}}, \end{aligned} \quad (3)$$

where in the last term, for  $\alpha < 0.5$  both  $\arccos[(2\alpha)^{-1}]$  in the numerator and  $\sqrt{4\alpha^2 - 1}$  in the denominator are purely imaginary so that  $F_l(\alpha)$  is real and positive for all  $\alpha$ . For screened short-range impurities, we have [22]

$$\begin{aligned} \sigma_s &= \frac{\sigma_0}{F_s(\alpha)}, \\ F_s(\alpha) &= \frac{\pi}{2} - \frac{32\alpha}{3} + 24\pi\alpha^2 + 320\alpha^3(1 - \pi\alpha) \\ &\quad + 256\alpha^3(5\alpha^2 - 1) \frac{\arccos[1/2\alpha]}{\sqrt{4\alpha^2 - 1}}, \end{aligned} \quad (4)$$

where similarly  $F_s(\alpha)$  is real and positive. Consistent with the physical picture outlined earlier, in the limit  $\alpha \rightarrow 0$ ,  $\sigma_l \sim \alpha^{-2}$  which describes the scaling of the Coulomb scattering matrix element, while for short-range scattering,  $\sigma_s \approx \text{const}[1 + (64/3\pi)\alpha]$  where increased screening of the potential by the carriers gives the leading order increase in conductivity. For the experimental values of  $\alpha$ , the full functional form of  $F_s$  and  $F_l$  should

be used [23]. Dashed lines in Figs. 3a-b show the theoretical expectations for  $\mu_{\text{sym}}$  and  $\sigma_{\text{sym}}$  for vacuum and ice on graphene in quantitative agreement with experiment.

Regarding the magnitude of the minimum conductivity, it was recently proposed [4] that one can estimate  $\sigma_{\text{min}}$  by computing the Boltzmann conductivity of the residual density  $n^*$  that is induced by the charged impurities. This residual density (i.e. rms density of electrons and hole puddles) has been seen directly in scanning probe experiments [24] and in numerical simulations [10]. We therefore use Eq. 3, but replace  $n$  with  $n^* = \langle V_D^2 \rangle / [\pi(\hbar v_F)^2]$  (where the angular brackets indicate ensemble averaging over configurations of the disorder potential  $V_D$ ) to give [4]

$$\begin{aligned} \sigma_{\text{min}} &= \frac{2e^2}{h} \frac{1}{F_l(\alpha)} \frac{n^*(\alpha)}{n_{\text{imp}}}, \\ \langle V_D^2 \rangle &= n_{\text{imp}}(\hbar v_F \alpha)^2 \int d\mathbf{q} \left( \frac{e^{-qd}}{q\epsilon(q)} \right)^2, \end{aligned} \quad (5)$$

where  $\epsilon(q)$  is the RPA dielectric function and  $d \approx 1\text{nm}$  is the typical impurity separation from the graphene sheet. The dominant contribution to both the disorder potential  $\langle V_D^2 \rangle$  and  $F_l(\alpha)$  is the Coulomb matrix element, giving  $n^* \sim n_{\text{imp}}\alpha^2$  and  $1/F_l(\alpha) \sim 1/\alpha^2$  so that to leading order,  $\sigma_{\text{min}}$  is unchanged by dielectric screening [25].

The experimental data also show a mobility asymmetry (between electrons and holes) of about 10 percent. Novikov [26] argued that for Coulomb impurities in graphene such an asymmetry is expected since electrons are slightly repelled by the negative impurity cen-

ters compared to holes resulting in slightly higher mobility for electrons (since  $V_{g,\min} > 0$ , we determine that there are more negatively charged impurity centers, see also Ref. [6]); and that for unscreened Coulomb impurities  $\mu_{\text{usc}}(\pm V_g) \sim [C_2\alpha^2 \pm C_3\alpha^3 + C_4\alpha^4 + \dots]^{-1}$ . From the magnitude of the asymmetry, we know that  $C_3\alpha^3 \ll C_2\alpha^2$ , but if we further assume that  $C_4\alpha^4 \ll C_3\alpha^3$  (although, in the current experiment, we cannot extract the value of  $C_4$ ), then including the effects of screening gives  $\mu_{\text{asym}} \sim \alpha/F_l(\alpha)$ .

In Table I we show all the experimental fit parameters and compare them to theoretical predictions. The quantitative agreement for  $\mu_{\text{sym}}$ ,  $\sigma_{\min}$  and  $\sigma_{\text{sym}}$  is already highlighted in Fig. 3, while we have only qualitative agreement for  $\mu_{\text{asym}}$ , probably because the condition  $C_4\alpha^4 \ll C_3\alpha^3$  does not hold in our experiments. There is no theoretical expectation of asymmetry in  $\sigma_s$ ; the experimental asymmetry (about 30 percent) could be explained by contact resistance [27] which we estimate to be a 20 percent correction to  $\sigma_s$  for our sample geometry.

In conclusion we have observed the effect of dielectric environment on the transport properties of graphene. The experiment highlights the difference between long-range and short-range potential scattering in graphene. The enhanced  $\mu_l$  (i.e. the slope of  $\sigma$  against density) and reduced  $\sigma_s$  (i.e. the constant conductivity at high density) are attributed to the decreased interaction between charged carriers and impurities and decreased screening by charge carriers, respectively, upon an increase in background dielectric constant with ice deposition in UHV. These variations quantitatively agree with theoretical expectations for the dependence of electron scattering on graphene's "fine structure constant" within the RPA approximation. This detailed knowledge of the scattering mechanisms in graphene is essential for design of any useful graphene device, for example, use of a high- $\kappa$  gate dielectric will increase the transconductance of graphene at the expense of linearity, an important consideration for analog applications. As demonstrated here, dielectric deposition only improved mobility by 30 percent, however the use of high- $k$  dielectric overlayers could significantly enhance this result.

We thank E. Hwang and E. Rossi for fruitful discussions. This work is supported by US ONR, NRI-SWAN and NSF-UMD-MRSEC grant DMR 05-20471.

---

[1] N. M. R. Peres, F. Guinea, and A. H. Castro Neto, Phys. Rev. B **72**, 174406 (2005).  
 [2] T. Ando, J. Phys. Soc. Jpn. **75**, 074716 (2006); K. Nomura and A. H. MacDonald, Phys. Rev. Lett. **96**, 256602 (2006).  
 [3] E. H. Hwang, S. Adam, and S. Das Sarma, Phys. Rev. Lett. **98**, 186806 (2007).  
 [4] S. Adam, E. H. Hwang, V. M. Galitski, and S. Das

Sarma, Proc. Natl. Acad. Sci. USA **104**, 18392 (2007).  
 [5] Y.-W. Tan *et al.*, Phys. Rev. Lett. **99**, 246803 (2007).  
 [6] J. H. Chen, C. Jang, S. Adam, M. S. Fuhrer, E. D. Williams, and M. Ishigami, Nature Physics **4**, 377 (2008).  
 [7] H. Min, R. Bistritzer, J. Su, and A. H. MacDonald, arXiv:0802.3462v1 (2008); Y. Zhang, V. W. Brar, F. Wang, C. Girit, Y. Yayon, M. Panlasigui, A. Zettl, and M. F. Crommie, arXiv:0802.4315v1 (2008).  
 [8] D. Jena *et al.*, Phys. Rev. Lett. **98**, 136805 (2007).  
 [9] T. Ando, A. B. Fowler, and F. Stern, Rev. Mod. Phys. **54**, 437 (1982); S. Das Sarma and B. Vinter, Phys. Rev. B **24**, 549 (1981).  
 [10] E. Rossi and S. Das Sarma, arXiv:0803.0963v1 (2008).  
 [11] K. S. Novoselov *et al.*, Nature **438**, 197 (2005).  
 [12] Y. Zhang *et al.*, Nature **438**, 201 (2005).  
 [13] Z. Jiang *et al.*, Phys. Rev. Lett. **98**, 197403 (2007).  
 [14] K. Bolotin *et al.*, Solid State Commun. **146**, 351 (2008); S. Adam and S. Das Sarma, *ibid.* **146**, 356 (2008).  
 [15] V. F. Petrenko and R. W. Whitworth, *The Physics of Ice* (Oxford University Press, Oxford, U.K., 1999).  
 [16] A. C. Ferrari *et al.*, Phys. Rev. Lett. **97**, 187401 (2006).  
 [17] M. Ishigami *et al.*, Nano Lett. **7**, 1643 (2007).  
 [18] P. C. Sanfelix *et al.*, Surface Science **532**, 166 (2003).  
 [19] P. A. Thiel *et al.* Surface Science Reports **7**, 211 (1987).  
 [20] The saturation behavior shown in Fig. 3 indicates that the ice film is continuous well before the formation of 6 full ice layers, and has reached a constant value of the dielectric constant. Bulk dielectric constant has been observed in ultrathin films of SiO<sub>2</sub>, see K. Hirose *et al.*, Phys. Rev. B **67**, 195313 (2003), and it is reasonable to assume that these ultrathin ice layers have the bulk dielectric constant of ice.  
 [21] S. Morozov *et al.*, Phys. Rev. Lett. **100**, 016602 (2008).  
 [22] S. Adam *et al.*, Physica E **40**, 1022 (2008).  
 [23] Results beyond the RPA approximation have been examined in A. V. Shytov *et al.*, Phys. Rev. Lett. **99**, 236801 (2007), R. R. Biswas *et al.*, Phys. Rev. B **76**, 205122 (2007), V. M. Pereira *et al.*, Phys. Rev. Lett. **99**, 166802 (2007), I. S. Terekhov *et al.*, Phys. Rev. Lett. **100**, 076803 (2008), M. S. Foster *et al.* Phys. Rev. B **77**, 195413 (2008) and M. Mueller *et al.*, arXiv:0805.1413v1 (2008). We believe that these effects are unobservable in the current experiment. Also M. Trushin *et al.* Europhys. Lett. **83**, 17001 (2008) consider a phenomenological Yukawa potential. Generally one uses a model Yukawa potential in studying systems where the microscopic nature of the screened potential is unknown which is not the case for graphene. For the Yukawa potential, we find  $F_y = \pi\alpha^2 + 8\alpha^3 - \pi\alpha\sqrt{1+4\alpha^2}$  which is qualitatively similar to Eq. 3.  
 [24] J. Martin *et al.*, Nature Physics **4**, 144 (2008).  
 [25] Estimating the charged impurity density  $n_{\text{imp}} \approx 5.5 \times 10^{10} \text{ cm}^{-2}$  (which is comparable to similar experiments [5, 6]) we find [4]  $\sigma_{\min}(\text{ice})/\sigma_{\min}(\text{vac}) \approx 6.66/6.72 \approx 0.99$ . The minimum conductivity (Fig. 3c) shows almost no variation with ice layers, in agreement with this theoretical expectation. We ignore quantum coherent effects such as localization (see e.g. I. Aleiner and K. Efetov, Phys. Rev. Lett. **97**, 236801 (2006)) which are not expected to be important at 77 K, and are not experimentally observed [5, 6, 11, 12, 21] down to 30 mK (see: Y.-W. Tan *et al.*, Eur. Phys. J. **148**, 15 (2007)).  
 [26] D. S. Novikov, Appl. Phys. Lett. **91**, 102102 (2007).  
 [27] B. Huard *et al.*, arXiv:0804.2040v1 (2008).